International Journal of Thin Films Science and Technology

http://dx.doi.org/10.18576/ijtfst/090102

Effect of TM (TM= Sn, Mn, Al) Doping on the Physical Properties of ZnO Thin Films Grown by Spray Pyrolysis Technique: A comparative Study

M. N. Amroun[1,*], *K. Salim*[1], *A. H. Kacha* [2] and *M. Khadraoui* [1]

[1] Laboratoire d'Elaboration et de Caractérisation des Matériaux, département d'électronique, Université Djilali Liabes, BP89, Sidi Bel Abbés 22000. Algeria
[2] Laboratoire de Micro-électronique Appliquée, Université Djillali Liabès de Sidi Bel Abbès, 22000 Sidi Bel Abbès, Algeria.

Received: 26 Aug. 2019, Revised: 10 Nov. 2019, Accepted: 20 Nov. 2019

Published online: 1 Jan. 2020

Abstract: ZnO:TM (TM=Sn, Mn, Al) thin films were successfully deposited on glass substrates using spray pyrolysis technique. X-ray analysis shows that ZnO:TM thin films crystallize in hexagonal structure with a preferred orientation of the crystallites along (002) direction and the crystallite size had increased with TM doping. The present study investigated the effect of TM type on the structural parameters. These films had direct band gap energy lying in the range of 3 – 2.25 eV and the average transmittance varied from 75 to 85 % with TM doping. The lowest observed figure of merit in the present study is 4.13×10^{-5} (Ω^{-1}) for AZO thin films. All the optical expected absorption capacity and photocurrent (j_{ph}) depend on the TM type. The optical constants, such as the urbach energy, effective mass of the carriers (m*), refractive index (n) and extinction coefficient (k), were also evaluated. The AZO thin films exhibited the lowest resistivity (1.79×10^{-1} Ω cm).
Keywords: ZnO, thin films, spray pyrolysis, Optical constants.

1 Introduction

Throughout the past decade, transparent conductive oxides (TCO) have grabbed the attention of various researchers because of their intriguing properties. Zinc oxide (ZnO), as one of them, is II–VI compound semiconductor, with a wide band gap of 3.37 eV and high exciton binding energy of 60 meV at room temperature [1].

In addition their electro-optical properties, high electro-chemical stability together with its natural abundance and non-toxicity [2] attracted their interest. They have been applied in several fields, such as optical bistability, spintronics and information technology devices including displays and wavelength selective applications [3, 4], UV-light emitting diode [5], gas sensors [6], field effect transistor [7], piezoelectric devices [8] and solar cells [9]. Transition metals (TM) have been used as successful doping materials for ZnO. The metal doping effectively improves the performance of ZnO nanostructures. Doping by metals, such as F, Cu, Ag, Ga, Al, In, Sn and Sb, is utilized to tailor the chemical, optical and the electrical properties of ZnO nanomaterials [10, 11].

Several methods including: thermal evaporation [12], gas condensation [13], hydrothermal synthesis [14], successive ionic layer adsorption [15], pulsed laser [16], chemical route [17], and spray pyrolysis [18, 19, 20] have been developed for the synthesis of zinc oxide systems.

Numerous dopants are used in the present paper. A change in dopant is significant for changing the physical properties of the material. For example, the prepared TM (TM =Sn, Mn and Al) doped ZnO thin films by spray pyrolysis method with a 4 at% doping level to understand and identify their enhanced optical and electrical properties with TM type. We have chosen 4 at% doping of the transition metal content for TM = Al, Mn and Sn because a doping level higher than 4 at% can change the structure of the material as well as the optical and electrical properties.

*Corresponding author E-mail: amroun_mn@yahoo.com

2 Experimental Details

The samples of pure ZnO, 4 at% Sn-doped ZnO, 4 at% Mn-doped ZnO and 4 at% Al-doped ZnO thin films (pure ZnO, TZO, MZO and AZO thin films respectively) were synthesized by spray pyrolysis technique onto microscope glass substrates of (75×25) mm^2. Pure ZnO thin films were prepared through dissolving 0.1 M of the $ZnCl_2$ powder in 100 ml of deionized water. To synthesize 4 at% Al, 4 at% Mn and 4 at% Sn-doped ZnO thin films, aluminium, manganese and tin doping were accomplished by adding 0.1 M aluminum chloride ($AlCl_3$), 0.1 M manganese chloride ($MnCl_2$) and 0.1 M tin chloride ($SnCl_2$) precursors into the solution, respectively. The substrate temperature was fixed at 350°C and controlled through a thermocouple (Chrome–Nickel). Compressed air of pressure 2 bars has been used as a carrier gas. Solution flow was 8 ml/min and spray nozzle to heating plaque distance was fixed to 29 cm. Moreover, the prepared solutions were immediately sprayed to avoid any possible chemical changes with time.

X-ray diffraction (XRD) patterns of the deposited films were recorded by Philips 1830 system using Cu Kα radiation (λ=1.546 Å) with 2θ in the range 25 – 65°. The optical measurements were carried out at room temperature in the wavelength range 250–2500 nm using an UV-Vis-NIR JASCO type V-570 double beam spectrophotometer. The electrical resistivity, carrier concentration and mobility were measured using an Automated Hall Effect System (ECOPIA HMS-5000) at room temperature and silver lacquer as contact.

3 Results and Discussion

3.1 Structural Properties

Fig 1.A. shows the X-ray diffraction (XRD) patterns of pure ZnO, TZO, MZO and AZO thin films. The obtained XRD patterns are quite similar, indicating that the ZnO films does not change in crystalline phase with the all dopants. The pure ZnO and ZnO:TM films are polycrystalline in nature with the diffraction planes of (100), (002), (101), (102),(110) and (103) that correspond to the purely hexagonal wurtzite structure (JCPDS card no: 65-3411 with lattice parameters a=3.249A° and c=5.20 A°). All the films exhibit strong orientation corresponding to (002) plane and confirmed the formation of stable hexagonal wurtzite crystal structure of ZnO. No other phase was detected, suggesting that the doping level of 4 at% is insufficient to allow the emergence of new phases. Moreover neither metallic Sn, Mn nor Al was observed in all the patterns exhibiting the successful dissolution of Sn, Mn and Al atoms into the crystal lattice of ZnO structure. Similar results were reported in the pieces of literature [23, 36]. Nevertheless, a slight shift of the (002) peak towards lower 2-theta degrees was observed (see Fig 1.B). The full-width-at-half maximum (FWHM) of the (002) peak increases with TM doping indicating a local distortion of the lattice because of some residual stress inside the nanoparticles. The hexagonal network lattice parameters 'a' and 'c'of the samples have been computed from the Bragg's hexagonal system formula [21] and are listed in Table 1.

$$\frac{1}{d_{hkl}^2} = \frac{4}{3}\left(\frac{h^2+hk+k^2}{a^2}\right) + \frac{l^2}{c^2} \quad (1)$$

Where d is interplanar spacing and (hkl) are the miller indices. The interplanar spacing d_{hkl} values of pure and TM doped ZnO thin films were calculated using the Bragg equation [26]. Table (1) exhibits that the values of the lattice parameters (a and c) are consistent with those of the JCPDS card no: 65-3411. The lattice constant (c) of the TZO and MZO films increases with TM (Sn and Mn) doping indicating the substitutional incorporation of of Sn^{+2} and Mn^{+2} ions in the ZnO lattice system, which leads to the expansion of the lattice since the ionic radius of Sn^{2+} (0.93 Å) and Mn^{+2} (0.80 Å) ions is larger than that of Zn^{2+} (0.74 Å). A. Goktas et al. and F.Z. Bedia et al. [22, 23] reported similar results of TM doped ZnO thin films grown by radio frequency magnetron sputtering and spray pyrolysis technique, respectively. On the other hand, compared to pure ZnO sample, c value slightly increases from 5.1768 A° to 5.19 A° for AZO thin films, This may occur because of the interstitial incorporation of Al^{+3} for Zn^{+2} sites in the ZnO lattice system since the ionic radius Al^{+3} ion (0.53 Å) is smaller than that of Zn^{2+} (0.74 Å) suggesting that Al^{+3} ions could not substitutionally enter in ZnO structure [24]. Moreover, the increase in the c-lattice parameters after 4 at.% Al doping occurs because the films are exposed to tensile strain along their c-axis. Furthermore, defects or incorporation of low amount of foreign atoms of 4 at% (not detected in XRD) may cause the change in the c values.

Zn-O bond length (L) changes because of Zn ions substitute with TM ions. Zn-O bond length L and u (the displacement of an atom from its lattice site) in ZnTMO structure were calculated using the following equations [35]:

$$L = \sqrt{\left(\frac{a^2}{3}\right) + c^2 * (0.5-u)^2} \quad (2)$$

$$u = \left(\frac{a^2}{3*c^2}\right) + \frac{1}{4} \quad (3)$$

Where, c and a are lattice constants of ZnO films. According to **Table 1**, with TM incorporation, the locality of the atom and its displacement in ZnTMO structures exhibited a fluctuation tendency. **Fig 2** depicted the variation of the lattice parameter (c) and Zn-O bond lengths (L) as function of TM doping. (c) lattice parameter and Zn-O bond length (L) showed an increment with TM incorporation. Stress and microstrain caused this fluctuation.

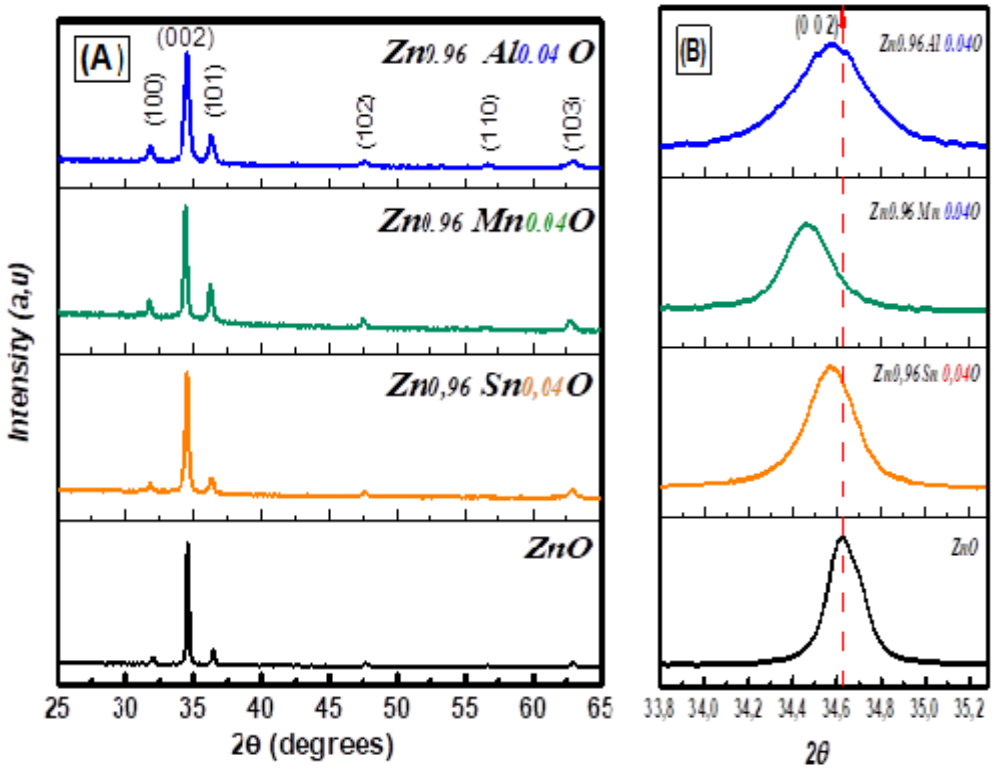

Fig. 1: XRD patterns of pure ZnO, TZO, MZO and AZO thin films.

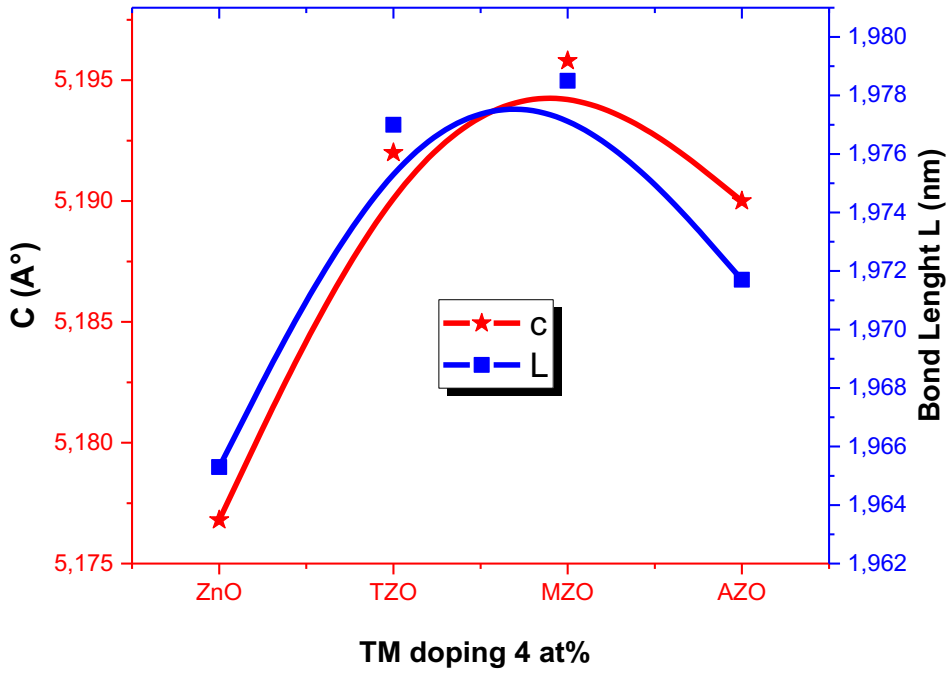

Fig.2: variation of (c) values and Zn-O bond lengths (L) in ZnO:TM structures.

Table 1: Summary of structural parameters of pure ZnO, TZO, MZO and AZO thin films.

Samples	Lattice constants (Å)		$d_{(0\,0\,2)}$ (Å)	FWHM (0 0 2) Peak (2θ)°	TC (0 0 2) texture coefficient	L (nm)	u (nm)
	a	c					
Pure ZnO	3.2283	5.1768	2.588	0.202	3.98	1.965	0.3796
TZO	3.2520	5.1920	2.596	0.2828	3.92	1.977	0.3808
MZO	3.2457	5.1958	2.597	0.2858	3.46	1.979	0.3801
AZO	3.2400	5.1900	2.592	0.404	3.38	1.971	0.3799

The texture coefficient (TC) for the preferred orientation of ZnO:TM thin films was estimated based on the following relation **[**25**]:**

$$TC_{(101)} = \frac{I_{(101)}/I^0_{(101)}}{(1/N)\sum_n I_{(hkl)}/I^0_{(hkl)}} \quad (4)$$

Where, I (hkl) is the measured relative intensity of a plane (hkl). I° (hkl) is the standard intensity of the plane (hkl) taken from the JCPDS data, N is the reflection number and 'N' is the number of diffraction peaks. The calculated texture coefficients TC are summarized in **Table 1**.

A sample with randomly oriented crystallite yields TC (h k l) = 1, However, if this value is higher than unity, the abundance of grains orients along a particular plane. In the present study, TC (002) value is 3.98 for pure ZnO thin films indicating a preferred orientation. However, the TC (002) value reduces for TZO, MZO and AZO films with TM doping suggesting that more randomly oriented grains, which lead to the degradation in the crystal quality of the ZnO films, are formed. For more illustration of the effect of TM doping on the structure of the ZnO crystals grown by spray pyrolysis technique, the crystallite size was calculated for preferential orientations using Scherer's equation. In addition, structural defects, such as micro-strain (ε), dislocation density (δ), stacking fault (α*) and Stress (σ^*) were calculated using the following relations **[26]**:

$$D = (0.9.\lambda)/(\beta.cos\theta) \quad (5)$$

$$\varepsilon = \frac{\beta\cos\theta}{4} \quad (6)$$

$$\delta = \frac{1}{D^2} \quad (7)$$

$$\alpha^* = \left(\frac{2\pi^2}{45(3tan\theta)^{1/2}}\right)\beta \quad (8)$$

$$\sigma^* = -453.6 * 10^9\left(\frac{c-c_0}{c_0}\right) \quad (9)$$

λ is the wavelength of Cu-Ka radiation, θ is the Bragg angle and β is the full width at half maximum (FWHM) of the most intense diffraction peak and c_o is the parameter obtained from the JCPDS card no: 65-3411 data card. All the calculated crystalline parameters of the deposited films are regrouped in **Table 2.**

In Eqn (9), the negative sign corresponds to the compressive stress. The positive stress refers to tensile stress **[**35**]**. Total stress consists of internal stress which includes defects and impurities, and external stress resulted from the lattice mismatch between substrate and film. **Table 2** exhibits that the obtained values of the stress of all the films are positive sign demonstrating that the thin films are in a state of tensile stress. D. Akcan et al. **[**35**]** had a similar observation of the ZnO films synthesized by the sol-gel technique.

The pure ZnO thin films exhibit the crystallite size of ~ 45.79 nm with FWHM of 0.202°, but TZO, MZO and AZO films exhibit smaller crystallite size of 32.69, 32.35 and 22.89 nm with FWHM of 0.2828, 0.2858 and 0.4040°, respectively. The large FWHM values of TZO, MZO and AZO films, compared with pure ZnO nanostructures, might be attributed to an decrement in the degree of polycrystallinity of the films. **Table 2** shows that the AZO films have the highest values of strain, dislocation density and stacking fault.

Fig. 3 shows the influence of ZnO doping with TM (Sn, Mn and Al) elements on the crystallite size, texture coefficient, and the corresponding micro-strain as well as stacking fault. It also reveals that the incorporation of TM content in ZnO films results in a decrease in the crystallite size associated with an increase in the micro-strain and the stacking fault. The obtained value of crystallite size of pure ZnO is consistent with that obtained by **[**23**].** In addition, the texture coefficient has a proportional relationship with the crystallite size and an inversely proportional relation with the structural defects. This results indicate that TM doping affects the structural properties of ZnO films.

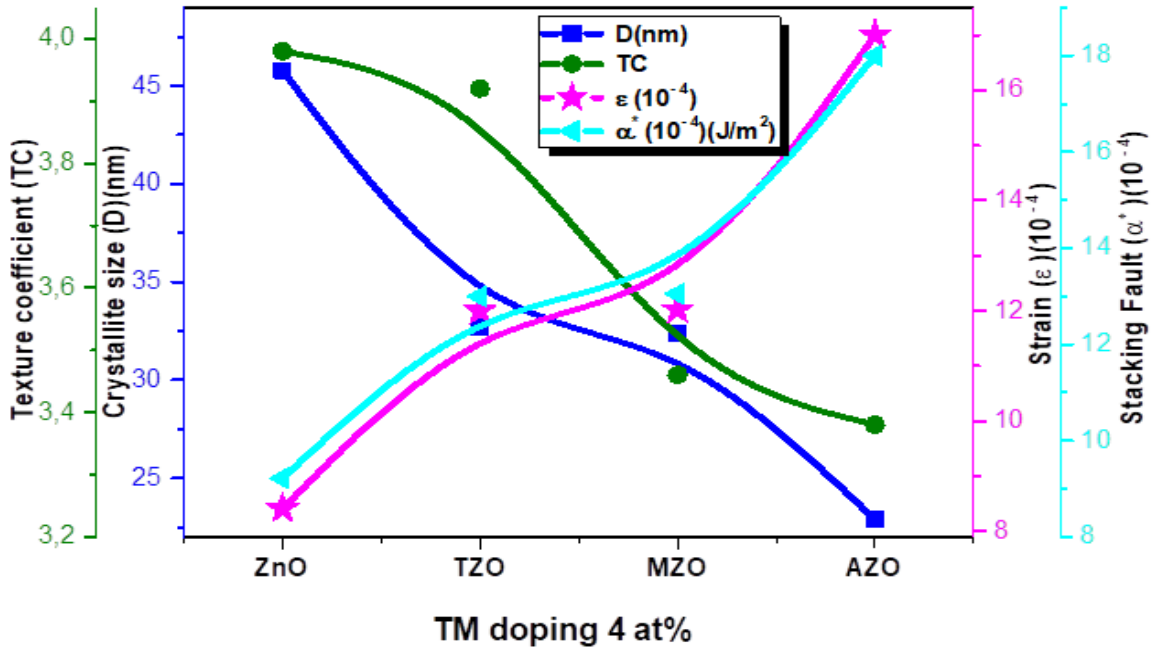

Fig. 3: the average crystallite size, texture coefficient (TC), micro-strain (ε) and Stacking fault (α^*) of the pure ZnO, TZO, MZO and AZO thin films.

3.2 Optical Properties

Optical transmittance properties of the deposited films are measured using UV-Vis-NIR JASCO spectrophotometer in wavelength range 250-2500 nm. In **Fig. 4,** we have regrouped the transmittance and reflectance spectra of undoped ZnO and TM-doped ZnO thin films. The transmittance spectra of the films indicate a sharp absorption edge in the wavelength range 310-380 nm. The position of this edge changes with TM doping. All films exhibit a large transmittance in the order of 80% and reflectance less than 12% in the Vis-NIR range. It shows that, the average transmittance increased from 75% for undoped ZnO films to 85% with Sn doping in the visible range, while the reflectance decreased from 9% to 3%. Sn doping slightly enhances the transmittance of the ZnO films indicating good incorporation of the Sn dopant in the ZnO lattice structure. H. Aydin et al. [36] observed similar results of Sn doped ZnO films prepared by spray pyrolysis method.

Thickness (d) of the deposited films was defined by the the spPS (seed preprocessing Pattern search) technique [27]. Thickness of the pure ZnO, TZO, MZO and AZO thin films was 210 nm, 223 nm, 192 nm and 178 nm, respectively.

The optical band gap of the films is calculated by Tauc plot [26, 28]. According to Tauc plot as shown in **Fig. 5,** the band gap of pure ZnO, TZO, MZO films was 3, 3.25, 3.17 and 3.08, respectively. The optical band gap increases with TM doping, reaching a maximum of about 3.25 eV for TZO films. This value is consistent with the values reported by Bedia et al. [23] for Sn doped ZnO thin films grown by spray pyrolysis method.

The band gap enlargement with TM doping can be attributed to the Burstein Moss shift: the doping creates degenerate energy levels with band filling that causes the Fermi level to move above the conduction band gap edge. This phenomenon induces an increases in the band gap with doping concentration [23, 29].

The increase of the band gap can also be attributed to the decrease in the network disorder (Urbach energy) because of TM incorporation in the film network as shown in **Fig. 6.**

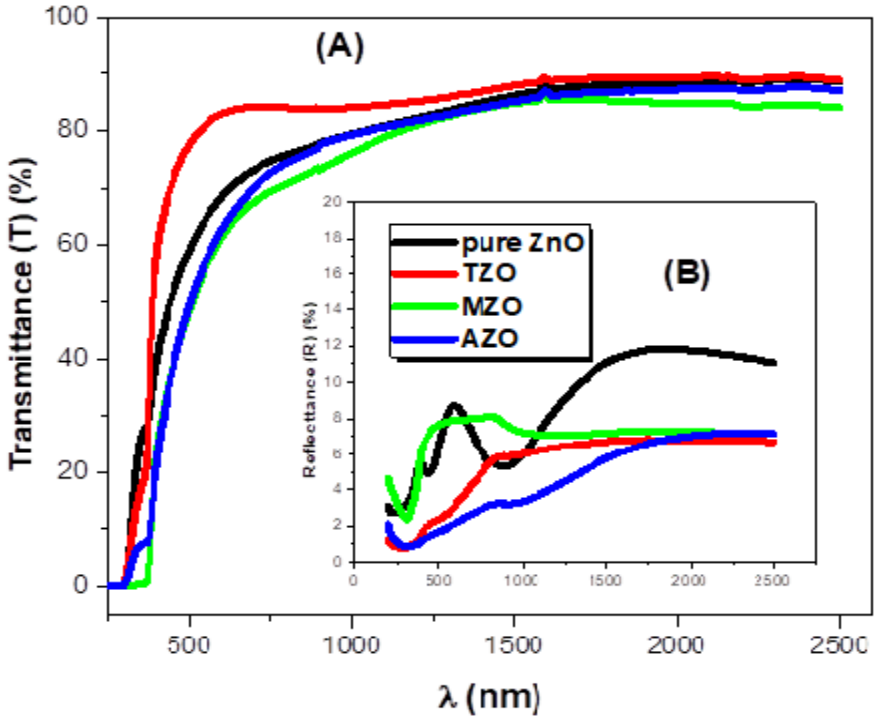

Fig 4: (A) Optical Transmission T, (B) Reflectance R spectra of pure ZnO, TZO, MZO and AZO Thin films.

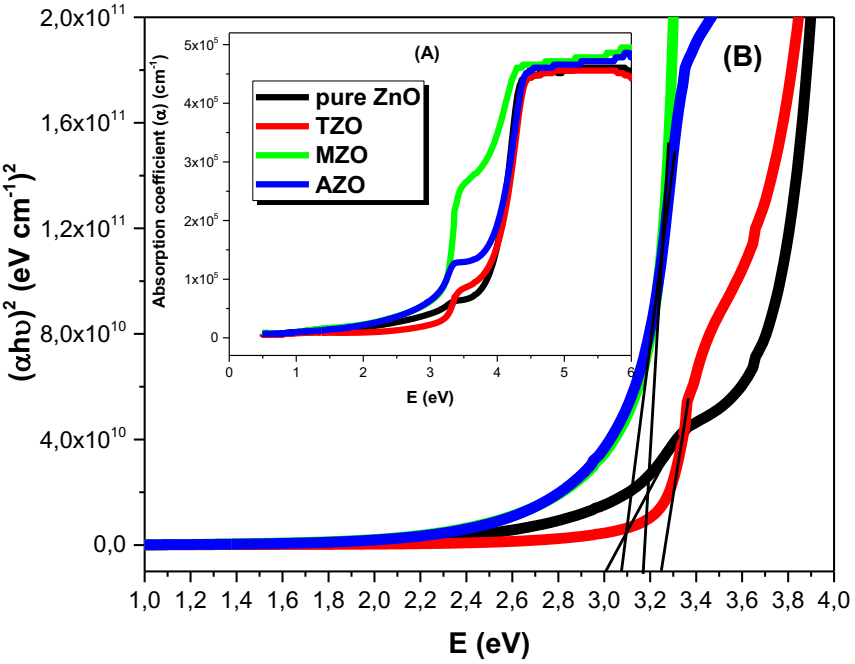

Fig 5: (A) absorption coefficient, (B) plot $(\alpha h\upsilon)^2$ versus energy (E) of pure ZnO, TZO, MZO and AZO thin films.

The disorder is also known as band tail width or Urbach energy. It is often interpreted as the width of the tail of localized states in the band gap. The Urbach energy can be easily estimated from the slope of the plot of ln (α) as a function of photon energy using the following formula **[**30**]**

$$\alpha = \alpha_0 \exp\left(h\upsilon/E_u\right) \quad (10)$$

α_0 is a constant and Eu denotes the Urbach energy. The obtained values are illustrated in **Table 3.** In **Fig. 6**, we have plotted the variation of the of Urbach energy together with optical band gap energy of the deposited films. It indicates, that the optical band gap variation is opposite to the disorder variation suggesting that the optical gap is controlled by the Urbach energy in the film network. The reduction of the urbach energy of ZnO films with TM doping could be attributed to the incorporation of TM atoms in ZnO structure. The potential barrier of grain boundary decreases because of the increase in carrier concentration caused by TM-doping. This rises the reduction in the resistivity of the ZnO:TM samples **[**24,31**],** which is also an evident from electrical measurements (see **Table 4**). The obtained value of urbach energy of pure ZnO thin films is consistent with that reported the pieces of in literature **[**39**]** of pure ZnO thin films prepared by spray pyrolysis method.

The effective mass of the carriers (m*) at the Fermi level of the samples was estimated using the following relations **[**40**]**

$$\mathrm{E} = \left[\frac{\mathrm{h}^2}{8\pi^2 \times m^*}\right] \mathrm{K}^{*2} \quad (11)$$

$$K^* = \frac{2\pi}{\lambda_a} = \frac{2\pi \times E_a}{hc} \quad (12)$$

E is the incident photon energy (hυ), h denotes the Planck constant, c is the speed of light, K^* denotes the wave number, Ea is the absorption energy of the material and m_e denotesthe electron of masse (9.11×10^{-31} Kg). The effective mass of the carriers (m*) of the samples was evaluated using the slope of the linear part of the variation of photo energy E as a function of square of the wave number K^{*2} of the films as shown in **Fig 7.** The calculated effective mass of the carriers m* of the deposited films is presented in **Table 3**. The evaluated effective mass of the increased from 1.86×10^{-31} Kg (0.204 m_e) for pure ZnO films to a maximum value of 2.18×10^{-31} Kg (0.239 m_e) for AZO films. The obtained effective mass values are in agreement with the data reported by W. S. Baer **[**32**]** and M. Oshikiri et al. **[**33**]**.The extrapolation of the linear portion of the plot onto the energy axis gives an optical band gap of the pure ZnO thin films as 2.998 eV (see **Fig 7**), which is comparable with the value obtained from the optical absorption measurements 3 eV.

The expected absorption capacity and photocurrent of the undoped and TM doped ZnO thin films were defined using the measured absorption coefficient data. The thickness-dependent absorbed photon fraction and the photocurrent of the films are calculated by the following relations **[**26, 34**]**

$$Absorbed\ photon\ fraction = \frac{\int_{300\ nm}^{\lambda g} F(\lambda)(1-\exp(-\alpha(\lambda)d))\,d\lambda}{\int_{300\ nm}^{\lambda g} F(\lambda)\,d\lambda} \quad (13)$$

$$J_{ph}(d) = q \times \int_{300\ nm}^{\lambda g} F(\lambda)(1-\exp(-\alpha(\lambda)d))\,d\lambda \quad (14)$$

$\alpha(\lambda)$ is the wavelength-dependent optical absorption coefficient of the film, $F(\lambda)$ denotes the AM1.5G photon flux, q is the electron charge and the wavelength $\lambda_g = hc/E_g$.

Fig 8 (A and B) illustrates the variation of the photocurrent and the absorbed photon fraction against thin film thickness of the deposited thin films. In the present study, the average photocurrent and the absorbed photon fraction of the pure ZnO are approximately 32 (mA/cm^2) and 0.98 for layer thickness greater than 1000 nm. However, they increase or decrease based on TM dopant type. Photocurrent and the absorbed photon fraction of the ZnO films increased gradually for AZO and MZO thin films and then decreased with Sn doping. Reduction in the photocurrent and the absorbed photon fraction of the TZO films compared to that of the undoped ZnO film can be correlated to the higher average transmittance of 85% in the visible range and the larger band gap 3.25 eV. Accordingly, the increase or decrease in the photocurrent and the absorbed photon fraction might be related to the compositional modifications due to the different TM dopants, which rise or reduce the optical quality of the films.

In solar cell applications, figure of merit (Φ_{TC}) plays a resoluble role and it is a good proof to define the quality of transparent conducting films. In this application, the optical transmittance and electrical conductivity are required to be as high as possible. The interrelationship between transmission and conductivity is expressed by the figure of merit (ϕ). Haacke's quality factor for the films is defined as **[**37**]**

$$\Phi_{TC} = \frac{T^{10}}{R_{sh}} \quad (15)$$

Where T^{10} is the transmittance at λ=average of (200–2500 nm) and R_{sh} is the sheet resistance. The figure of merit values calculated for pure ZnO, TZO, MZO and AZO thin films were equal in order of 3.23×10^{-8}, 2.79×10^{-7}, 7.62×10^{-9} and 4.13×10^{-5} (Ω^{-1}), respectively (**Table 3)**. The value of figure of merit obtained for MZO thin film is very low because of the high value of sheet resistance (see **Table 4**). The figure of merit value obtained for AZO film is 4.13×10^{-5} (Ω^{-1}), and it is consistent with the reported values in the piece of literature **[**38**].**

The refractive index of the semiconductor is a measure of its transparency to incident spectral radiation. The refractive index of the film was defined by **[**41**]**

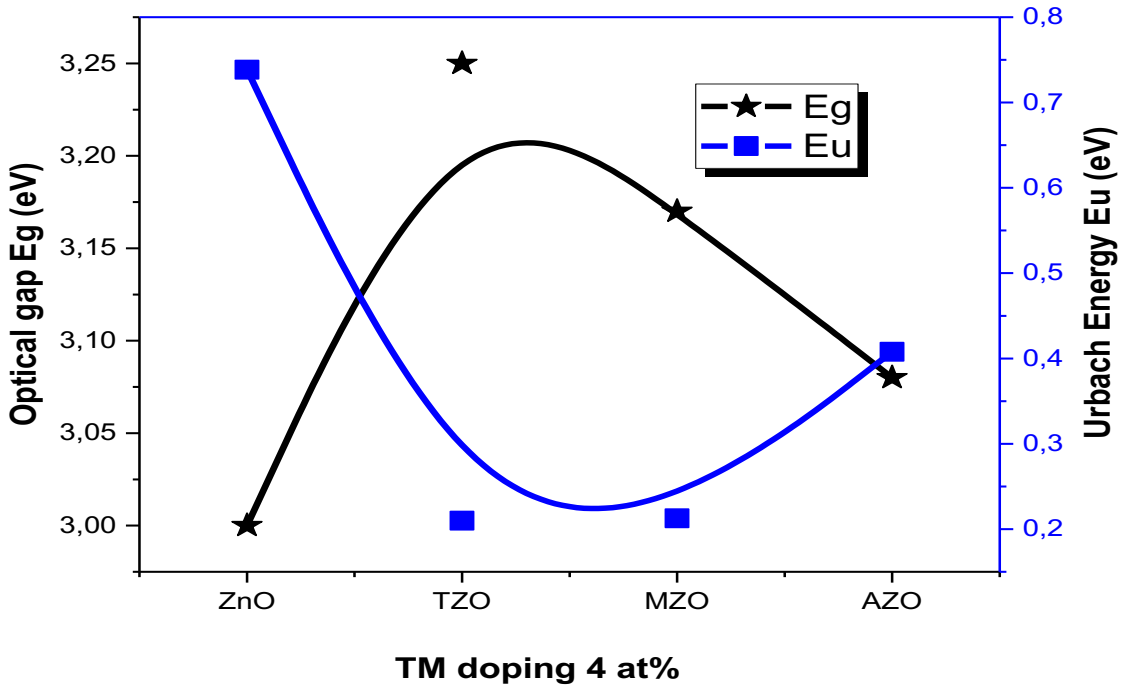

Fig. 6: Optical gap and Urbach's energy of the pure ZnO, TZO, MZO and AZO thin films.

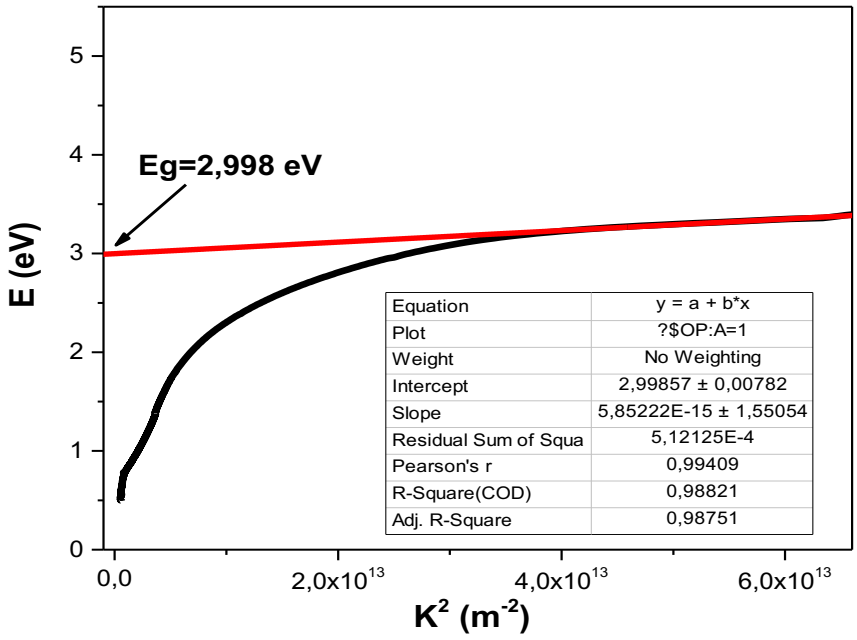

Fig. 7: Photon energy E as a function of K^2 of pure ZnO thin films.

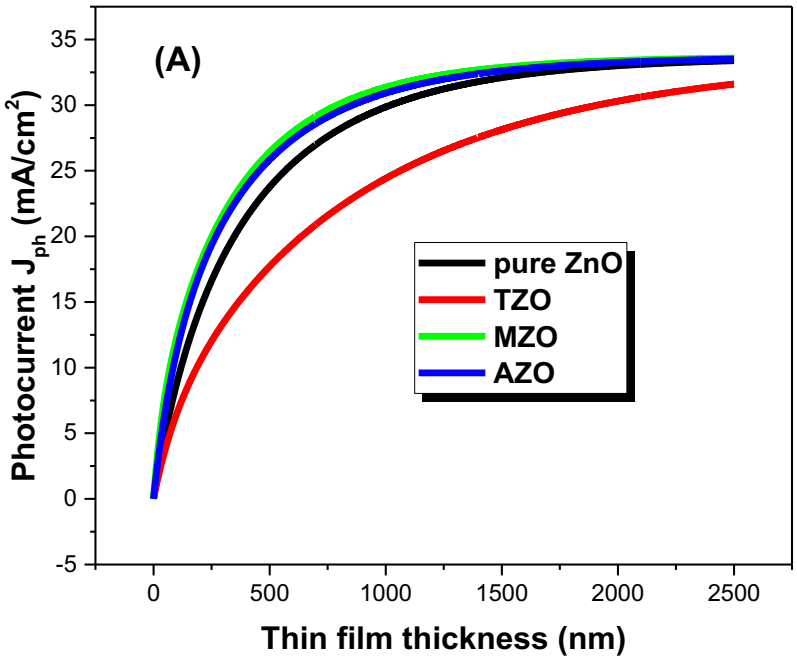

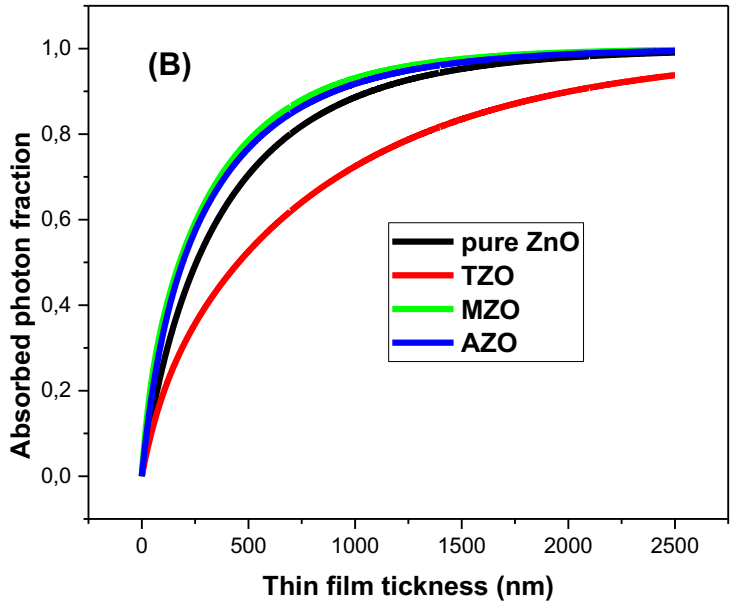

Fig. 8: (A) Photocurrent and (B) Absorbed photon fraction versus layer thickness of pure ZnO, TZO, MZO and AZO thin films.

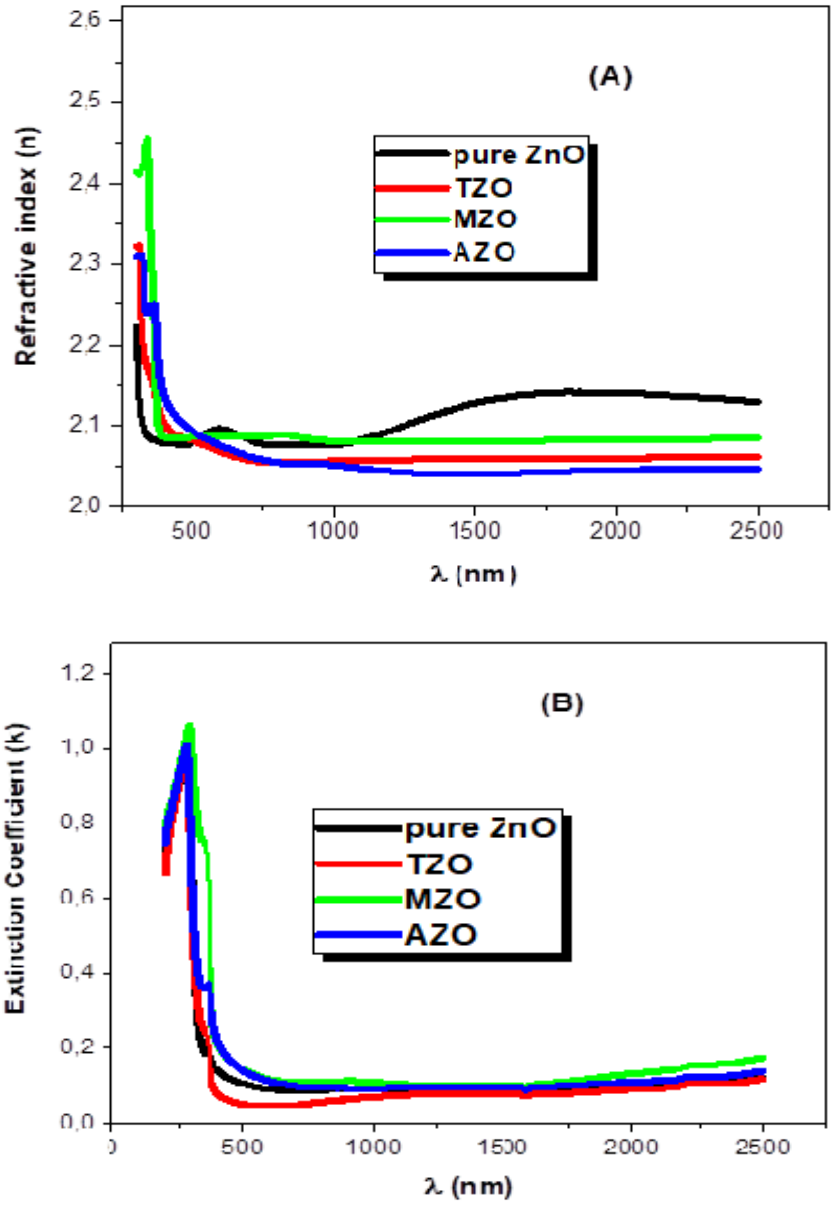

Fig. 9: (A) refractive index n, (B) extinction coefficient of pure ZnO, TZO, MZO and AZO thin films.

Table 2: the results and determinations using XRD data of pure ZnO, TZO, MZO and AZO thin films.

Samples	Crystallite size (D) (nm)	Dislocation Density(δ) (10^{-4} line/nm^2)	Strain (ε) (10^{-4})	Stacking fault (α*) (10^{-4} J /m^2)	Stress (σ*) (10^9 N/m^2)
Pure ZnO	45.79	4.76	8.41	9.22	2.49
TZO	32.69	9.35	12	13	1.16
MZO	32.35	9.55	12.02	13.05	0.83
AZO	22.89	19	17	18	1.34

Table 3: Optical parameters of pure ZnO, TZO, MZO and AZO thin films.

Samples	Eg (eV)	Eu (eV)	m* (Kg)	m*/m$_e$	Φ_{TC} (Ω^{-1})
Pure ZnO	3	0.73	1.86×10^{-31}	0.204	3.23×10^{-8}
TZO	3.25	0.20	2.10×10^{-31}	0.230	2.79×10^{-7}
MZO	3.17	0.21	1.90×10^{-31}	0.209	7.62×10^{-9}
AZO	3.08	0.40	2.18×10^{-31}	0.239	4.13×10^{-5}

Table 4: The Hall Effect results of the pure ZnO, TZO, MZO and AZO thin films.

Samples	Resistivity (ρ) (Ωcm)	Mobility (cm^2/VS)	Carrier Concentrations (cm^{-3})	Hall Coefficient (cm^3/C)	Sheet Resistance (Rsh) (Ω/sq)
Pure ZnO	$1.92 \times 10^{+2}$	3.32	$-9.74 \times 10^{+15}$	$-6.40 \times 10^{+2}$	$9.63 \times 10^{+6}$
TZO	$2.50 \times 10^{+1}$	0.17	$-2.49 \times 10^{+18}$	-4.46	$1.25 \times 10^{+6}$
MZO	$2.20 \times 10^{+2}$	1.73	$-1.62 \times 10^{+16}$	$-3.83 \times 10^{+2}$	$2.20 \times 10^{+7}$
AZO	1.79×10^{-1}	0.55	$-6.33 \times 10^{+19}$	-9.86×10^{-2}	$5.97 \times 10^{+3}$

$$n = \frac{1+R}{1-R} + \sqrt{\frac{4R}{(1-R)^2} - k^2} \qquad (16)$$

Where R is the reflectance at room temperature, λ is the wavelength of the incident photon and $k = \frac{\alpha\lambda}{4\pi}$ is the extinction coefficient.

Figs. 9 (**A and B**) presents the refractive index and extinction coefficient of the deposited thin films depending on wavelength range from 300 nm to 2500 nm, respectively.

In the present study, the average n value of the deposited films is approximately 2.07 in the visible range, which is consistent with the reported results for the ZnO films **[**22**].** However, the refractive index and the extinction coefficient for all samples reduce when the wavelength increase. This phenomenon is attributed to light scattering and absorbance reduction. The refractive index in Vis-NIR region of all films diminishes with TM doping, but the extinction coefficient decreases with Sn doping.

3.3 Electrical Study

The Hall Effect measurements of the pure ZnO, TZO, MZO and AZO thin films have been investigated at room temperature. Electrical resistivity, mobility, Bulk concentration, Hall coefficient and sheet resistance are shown in **Table 4**. The negative sign of the Hall coefficients observed for all the ZnO samples indicates that they are on n-type materials.

High value of the resistivity was observed for undoped ZnO films of 1.92 10^{+2} Ωcm. The carrier concentration increased from 9.74 10^{+15} cm^{-3} for pure ZnO films and reached the maximum of 6.33 10^{+19} (cm^{-3}) for AZO films. Then, it decreased to a value of 2.49 10^{+18} cm^{-3} for TZO films. In contrast the resistivity decreased with TM doping and reached a minimum of 1.79 10^{-1} Ωcm for AZO films. Then, it increased to 2.50 10^{+1} Ωcm for TZO films. The mobility values of the ZnO films decreased with TM doping because of the decrease in the crystallinity of the films.

4 Conclusion

In this paper, we have analyzed the TM (Sn, Mn and Al) doping on some structural, optical and electrical properties of sprayed ZnO films. Undoped and TM doped ZnO nanocrystalline thin films were deposited on glass substrate by spray pyrolysis technique. The single hexagonal wurtzite phase with the preferentially oriented towards (002) direction for all the films was obtained. The optical band gap of the films increased with TM doping. The optical parameters such as transmittance (T), reflectance (R), the expected absorption capacity, photocurrent (j_{ph}) and figure of merit (Φ_{TC}) counted on the TM type. The refractive index (n) and extinction coefficient (k) values varied with TM doping. These observations suggested that one can define the right TM type which involves higher optical and electrical constants. The investigated electrical properties of TM-doped ZnO thin films have demonstrated that TM doping improved the carrier concentration and resistivity of ZnO thin films. This result is very significant because a cost-effective and simple spray pyrolysis technique has been used to prepare such doped oxides and to facilitate valorisation of the prepared films in several optoelectronic and solar cell applications.

References

[1] A.A. Othman, M.A. Osman , E.M.M. Ibrahim , Manar A. Ali , A.G. Abd-Elrahim, Materials Science and Engineering, **B 219**, 1–9, 2017.

[2] K.K. Nagaraja , S. Pramodini , A. Santhosh Kumar , H.S. Nagaraja , P. Poornesh, Dhananjaya Kekuda, Optical Materials., **35**, 431–439, 2013.

[3] H. Hartnagel, A.L. Dawar, A.K. Jain, C. Jagadish, Semiconducting Transparent Thin Films, IOP Publishing, Bristol and Philadelphia., 1995.

[4] S.J. Pearton, D.P. Norton, Y.W. Heo, L.C. Tien, M.P. Ivill, Y. Li, B.S. Kang, F. Ren, J. Kelly, A.F. Hebard, J. Electron. Mater., **35**, 862–868, 2006.

[5] Q. Yang, Y. Liu, C. Pan, J. Chen, X. Wen, Z.I. Wang, Nano Lett., **13,** 2282, 2013.

[6] A. Wei, L. Pan, W. Huang, Mater. Sci. Eng. B., **176**, 1409, 2011.

[7] R.C. Hoffman, P. Atanasowa, S. Dilfer, J. Bill, J.J Schneider, Phys. Status Solidi A, **208**, 1983, 2011.

[8] Z.L. Wang, MRS Bull., **37**, 814, 2012.

[9] N. Sekine, C.-H. Chou, W.L. Kwan, Y. Yang, Org. Electron. 10 (8) (2009) 1473– 1477.

[10] S. Ilican, Y. Caglar, M. Caglar, F. Yakuphanoglu, Appl. Surf. Sci. **255**, 2353–2359, 2008.

[11] X.B. Wang, C. Song, K.W. Geng, F. Zeng, F. Pan, Appl. Surf. Sci., 253, 6905–6909, 2007.

[12] S.C. Navale, I.S. Mulla, Mater. Sci. Eng., **C 29**, 1317–1320, 2009.

[13] W. Jin, I. K. Lee, A. Kompch, U. Dörfler, and M. Winterer, J. Eur. Ceram. **Soc.27**, 4333-4337, 2007.

[14] C.H. Lu, W.J. Hawang, S.V. Godbole, J. Mater. Res., **20** , 464, 2005.

[15] S.T. Shishiyanu, T.S. Shishiyanu, O.I. Lupan, Sens. Actuators., **B 107**, 379–386, 2005.

[16] E. Holmelund, J. Schou, S. Tougaard, N.B. Larsen, Appl. Surf. Sci., **197–198**, 467–471, 2002.

[17] M.R. Vaezi, S.K. Sadrnezhaad, Mater. Sci. Eng., **B 141**, 23–27, 2007.

[18] S. Aksoy, Y. Caglar, S. Ilican, M. Caglar, Opt. Appl. **40** 7–14, 2010.

[19] N. Kawamoto, M. Fujita, T. Tatsumi, Y. Horikoshi, Jpn. J. Appl. Phys. 42, 7209–7212, 2003.

[20] Preetam. Singh, Ajay. Kaushal, Davinder. Kaur, J. Alloys Compd., **471**, 11–15, 2009.

[21] M.N. Amroun, M. Khadraoui, R. Miloua, Z. Kebbab, K. Sahraoui. Optik., **131,** 152–164, 2017.

[22] A.Goktas ,F.Aslan, A.Tumbul, S.H.Gunduz, Ceramics International., **43**, 704-713, 2017.

[23] F.Z. Bedia, A. Bedia, M. Allerie, N. Maloufi, B. Benyoucef. Energy procedia.,**74** 539-546, 2015.

[24] S. Yılmaz, Y. Atasoy, M. Tomakin, E. Bacaksız, Superlattices and Microstructures., **88**, 299-307, 2015.

[25] O. Lupan, T. Pauporte, L. Chow, B. Viana, F. Pelle, L.K. Ono, B. Roldan Cuenya, H. Heinrich, Applied Surface Science **256**, 1895–1907, 2010.

[26] M.N. Amroun, M. Khadraoui,Optik., 184, 16-27, 2019.

[27] R. Miloua, Z. Kebbab, F. Chiker, K. Sahraoui, M. Khadraoui, N. Benramdane, Opt. Lett., 37, 4, 2012.

[28] J. Tauc, R. Grigorovic, A. Vancu, Phys Stat Sol., **15**, 627–637, 1966.

[29] Burstein E. Phys.Rev., **93** ,632, 1954.

[30] M.N. Amroun, M. Khadraoui, R. Miloua, N. Benramdane, K. Sahraoui, Z. Kebbab, journal pf optoelectronique and advanced materials., **19**, 771 – 777, 2017.

[31] E. Bacaksiz, S. Aksu, S. Yılmaz, M. Parlak, M. Altunbas, Thin Solid Films., **518**, 4076-4080, 2010.

[32] W. S. Baer: Phys. Rev., **154**, 785, 1967.

[33] M. Oshikiri, Y. Imanaka, F. Aryasetiawan, G. Kido Physica B 298 (2001) 472}476

[34] R. Khadraoui, N. Miloua, A. Benramdane, K. Bouzidi, Mater. Chem. Phys., 1–7, 2015.

[35] D. Akcan, A. Gungor , L. Arda, Journal of Molecular Structure 1161 (2018) 299e305

[36] H. Aydin, H.M. El-Nasser, C. Aydin, Ahmed. A. Al-Ghamdi, F. Yakuphanoglu, Applied Surface Science., **350**, 109-114, 2015.

[37] M. Anitha, V. Tamilnayagam, N. Anitha, L. Amalraj, S. Gokul Raj, J. Mater.Sci.: Mater. Electron., **28**, 17297–17307, 2017.

[38] A. Bedia F. Z.Bedia, M. Aillerie, N. Maloufi, Superlattices and Microstructures., **111**, 714-721, 2017.

[39] A. Bedia F. Z.Bedia, M. Aillerie, N.Maloufi, B. Benyoucef .Energy Procedia., 50603-609, 2014.

[40] N. Koteeswara Reddy, K.T. Ramakrishna Reddy, Materials Research Bulletin 41 (2006) 414–422

[41] A.Mary Saroja, I.Kartharinal Punithavathy, S.Johnson Jeyakuma, S.Joshua Gnanamuthu, A.R.Balu, Optik, **130** 245-254, 2017.

[42] Amroun MN, Khadraoui M. Int J Numer Model. 2019;e2617. https://doi.org/10.1002/jnm.2617.